Langmuir

ARTICLE

pubs.acs.org/Langmuir

Light-Activated Covalent Formation of Gold Nanoparticle−Graphene and Gold Nanoparticle−Glass Composites

Hossein Ismaili,[†] Dongsheng Geng,[‡] Andy Xueliang Sun,[‡,§] Trissa Trisevgeni Kantzas,[‡] and Mark S. Workentin*[,†,§]

[†]Department of Chemistry, The University of Western Ontario, London, Ontario N6A 5B7, Canada

[‡]Faculty of Engineering, Spencer Engineering Building, The University of Western Ontario, London, Ontario N6A 5B9, Canada

[§]Centre for Advanced Materials and Biomaterials Research, The University of Western Ontario, London, Ontario, Canada, N6A 3K7

Supporting Information

ABSTRACT: Monolayer protected gold nanoparticles (AuNPs) modified with a 3-aryl-3-(trifluoromethyl)diazirine functionality at its terminus (Diaz-AuNPs, 3.9 nm) were prepared and irradiated in the presence of two very different substrates, reduced graphene and glass. Upon irradiation, the terminal diazirine group loses nitrogen to generate a reactive carbene at the interface of the AuNPs that can then undergo addition or insertion reactions with functional groups on the graphene or glass surfaces, leading to the formation of graphene−AuNP and glass−AuNP hybrids, respectively. The AuNP hybrids were characterized using TEM, XRD, XPS, AFM, and UV−vis spectroscopy. Control experiments done in the absence of irradiation demonstrate that carbene activation is required for incorporation of significant AuNP onto the materials. The AuNP hybrids are robust and stable to excessive washing and centrifugation supporting the covalent nature of the interaction between the AuNP and the graphene or silicate glass substrates. Because the formation of the composite is light activated, it lends itself to photopatterning; this application is demonstrated for making the glass−AuNP composites.

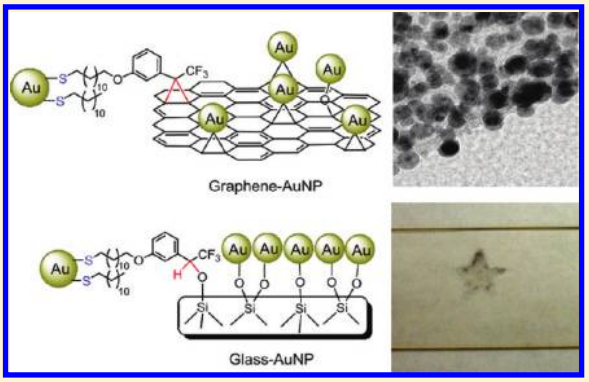

INTRODUCTION

The assembly and immobilization of metal nanoparticles on material surfaces is a primary step in engineering interparticle properties and in the development of new hybrid materials as sensing platforms.[1−3] When nanoparticles are organized in 2D or 3D networks, new collective optical, electronic, and magnetic properties are displayed by the ensembles of nanoparticles that are different as compared to those of their isolated counterparts. These collective properties have potential applications in biological and chemical sensing as well as in electronic, optoelectronic, and high-density information storage devices.[4−7] Most recently, interest has centered on hybrid materials based on gold nanoparticles (AuNPs), and deposition of AuNPs onto material surfaces has been extensively investigated for the following reasons: interparticle properties of AuNPs have potential applications in catalysis, sensing, as well as electronic and optoelectronic devices; incorporation of AuNPs can improve the physical and mechanical properties of materials; the combination of AuNPs with a host nanomaterial extends the possible uses of both by prosperous integration of the properties of the two components; defined patterned structures can be obtained by assembling AuNPs on a surface; and AuNPs are ideal candidates to study the interaction of material and biomaterial surfaces with metallic nanoparticles because there are conventional procedures to synthesize naked AuNPs or AuNPs with an organic monolayer bearing functional groups.[1−3,8−11]

The decoration of various materials with AuNPs including silicon oxide,[12,13] carbon nanotubes (CNTs),[14,15] graphene,[16,17] and diamond[18,19] has been demonstrated. The existing approaches for this decoration include covalent, noncovalent, and direct deposition of AuNPs.[12−19] In the latter approach, naked AuNPs (those not stabilized by a thiol monolayer) are formed directly on the surfaces usually via electrodeposition or in situ reduction of a gold salt. This approach has been used successfully; however, it requires more elaborate instrumentation for the controlled deposition of the AuNP and control over the core size of the AuNP is difficult.[12−15] The noncovalent approaches using monolayer-stabilized AuNP involve electrostatic, van der Waals forces, and $\pi-\pi$ stacking interactions between functionalities on the material surface and those on the monolayer of AuNPs to drive the formation of the hybrid structure. However, because of the relatively weak nature of these intermolecular (intermaterial) interactions, the resulting hybrid assemblies are not mechanically robust, and the AuNPs can be removed from the surface often by

Received: July 21, 2011
Revised: September 15, 2011
Published: September 20, 2011

simple washing.[8−11] The covalent attachment of AuNPs provides a method to prepare more robust hybrid structures with a designed preprepared AuNP core size. A typical strategy for covalent bonding of the AuNPs onto the surface involves carrying out a chemical reaction between terminal functional groups exposed on the monolayer of AuNPs with the functional groups accessible at the surface of the other material. This often requires preparing specific functionality on the AuNP and pretreatment of the material surfaces to find suitable reaction partners for the assembly of the composite.[2,7−11]

We recently reported an efficient protocol for the synthesis of covalently assembled AuNP hybrid materials that utilize photoinitiated carbene insertion/addition reaction between a carbene carrier, in this case AuNP, and surfaces with any X−H (X: O, N), C−H, or C═C functionality.[20−22] Specifically, we designed and prepared 3-aryl-3-(trifluoromethyl) diazirine-modified AuNPs (Diaz-AuNPs), which, when irradiated, yielded reactive carbene-modified AuNPs that were shown to react with the surface functionality of CNTs[21] and microdiamond,[22] leading to the production of desired AuNP−nanohybrids (CNT−AuNP and diamond−AuNP). Because of the inherent reactivity of the carbene-modified AuNP, we proposed in these initial communications that the protocol would be general, where the carbene generated would serve as the moiety to anchor essentially any additional functional group tethered to it for the modification of a host of material substrates. Indeed, Wildgoose and co-workers, who utilized our protocol for the attachment of ferrocene to CNT, have now demonstrated this.[23] Herein, we further demonstrate that the protocol can be extended and used for the fabrication of a broader range of AuNP-based hybrid materials as different as graphene and glass.

Graphene is a well-studied closely packed 2D nanomaterial composed of sp^2-bonded carbon atoms that has enormous potential for various applications as a promising building block of new hybrid materials.[24−26] Because of its unique physical, thermal, electrical, and mechanical properties, graphene has been investigated in many technological fields including nanoelectronics,[27] sensors,[28] biodevices,[29] batteries,[30] and drug delivery.[31] To further develop and explore advanced applications of graphene, the synthesis of graphene-based hybrid materials is a key requirement. Among graphene-based hybrid materials, graphene−AuNP hybrids[16,17] (graphene loaded with AuNPs) are the most studied, and their application in biosensors,[32] catalysis,[33] memory devices,[34] and photocatalytic degradation of organic compounds[35] has been demonstrated. Typically, in situ reduction of a gold salt on graphene oxide or a noncovalent assembly has been employed to obtain graphene−AuNP hybrids.[27−31] Besides the need for using only graphene oxide (not reduced graphene) and the small extent of AuNP loading, the lack of control over the AuNP size and the weak interactions between AuNPs and graphene limit the efficiency of these methods. Because of the high reactivity of carbenes for insertion into C═C frameworks, we demonstrate herein that our protocol of using photoinitiated carbene insertion reactions is efficient to produce robust covalently assembled graphene−AuNP hybrids with a high AuNP loading, which is an important consideration for most applications.

Glass slides, consisting mainly of silanol surface functionality, have been widely used in plasmonic nanoparticle-based sensors[36−39] and biochips, particularly DNA and protein biochips.[40,41] This is because of their low cost, transparency, and having a flat surface with functionalization capability. As a plasmonic nanoparticle, AuNPs have also been immobilized on glass slides to make a glass−AuNP hybrid. Detection of DNA hybridization,[42] label-free biosensing by surface plasmon resonance,[39] and patterning[43] are examples of applications of such glass−AuNP hybrids. Deposition of metal nanoparticles with premade core size or biological substrates onto glass slides requires functionalization of the surface with chemical groups. Often silanization of the surface hydroxyl groups is the initial step of functionalization of a glass surface. However, silanization is a sensitive reaction with a low yield and excessive polymerization often happens.[41] For the AuNP case, avoiding silanization can be achieved by generating reactive groups like carbene on the monolayer of AuNPs, which can then undergo reaction with hydroxyl groups at the surface of glass slides. In this Article, we demonstrate the ubiquitousness of the carbene−AuNP protocol for the fabrication of covalently assembled AuNP hybrids by extending our earlier work to the production of very different graphene−AuNP and glass−AuNP hybrids. The results in total confirm our suggestion that the photoinitiated carbene protocol is efficient for the covalent immobilization of AuNP onto essentially any material (with an organic functionality at the surface) because of the high reactivity of the carbene to both insertion and addition reactions with inherent chemical functionality.

EXPERIMENTAL SECTION

Commercial Solvents and Reagents Used. Deuterated chloroform ($CDCl_3$) and dichloromethane (CD_2Cl_2) (Cambridge Isotope Laboratories) were used as received. The compounds dodecanethiol, hydrogen tetrachloroaurate(III), tetraoctylammonium bromide (TOAB), 1,12-dibromododecane, 3-bromoanisole, *n*-butyllithium, hydroxylamine hydrochloride, (*N*,*N*-dimethylamino) pyridine, *p*-toluenesulfonylchloride, silver(I) nitrate, boron tribromide, potassium thioacetate, and acetyl chloride were used as received from the suppliers.

General Instrumentation. ^{1}H, ^{13}C, and ^{19}F NMR spectra were recorded on either a Varian Inova or a Mercury 400 spectrometer (^{1}H, 400 MHz; ^{13}C, 100 MHz; and ^{19}F, 376 MHz), and chemical shifts are reported in ppm relative to internal TMS (0.00 ppm) or the signals from the NMR solvent ($CHCl_3$, δ 7.26 ppm for ^{1}H NMR, δ 77.0 ppm for ^{13}C NMR; and $CFCl_3$, δ 0 ppm for ^{19}F NMR). Mass spectra and exact mass were recorded on a MAT 8200 Finnigan high-resolution mass spectrometer. Fourier transform infrared spectra were recorded on a Bruker spectrometer (FTIR, Bruker Tensor 27) and are reported in wavenumbers (cm^{-1}). The light source used for the photochemical reactions was a Hanovia medium pressure mercury lamp (PC 451050/616750, 450 Wage). Transmission electron microscopy (TEM) images were recorded on a Philips CM-10 TEM operating at 100 kV and FEI Tecnai G2 F20 operating at 200 kV. UV−vis absorption spectra were recorded on a Cary 100 spectrometer in spectroscopic grade THF and CH_2Cl_2. An Inel MPD (Multi-Purpose diffractometer) with a curved CPS 120 detector was used to collect X-ray powder diffraction data (XRD). The pattern was taken in the range of 5° and 120° 2θ with copper radiation. The XPS analyses were carried out with a Kratos Axis Ultra spectrometer using a monochromatic Al Kα source (15 mA, 14 kV). XPS can detect all elements except hydrogen and helium, probes the surface of the sample to a depth of 5−7 nm, and has detection limits ranging from 0.1 to 0.5 atomic percent depending on the element. The instrument work function was calibrated to give a binding energy (BE) of 83.96 eV for the Au $4f_{7/2}$ line for metallic gold, and the spectrometer dispersion was adjusted to give a BE of 932.62 eV for the Cu $2p_{3/2}$ line of metallic copper. The Kratos charge neutralizer system was used on all specimens. Survey scan analyses were carried out with an analysis area of 300 × 700 μm and a pass energy of 160 eV. High-resolution analyses were carried out with an analysis area of 300 × 700 μm and a pass energy of 20 eV. Spectra have been charge corrected to the main line of the carbon 1s spectrum

Scheme 1. Cartoon Illustration of the Carbene Insertion/Addition Approach Utilized for the Covalent Attachment of AuNPs onto Graphene and Glass

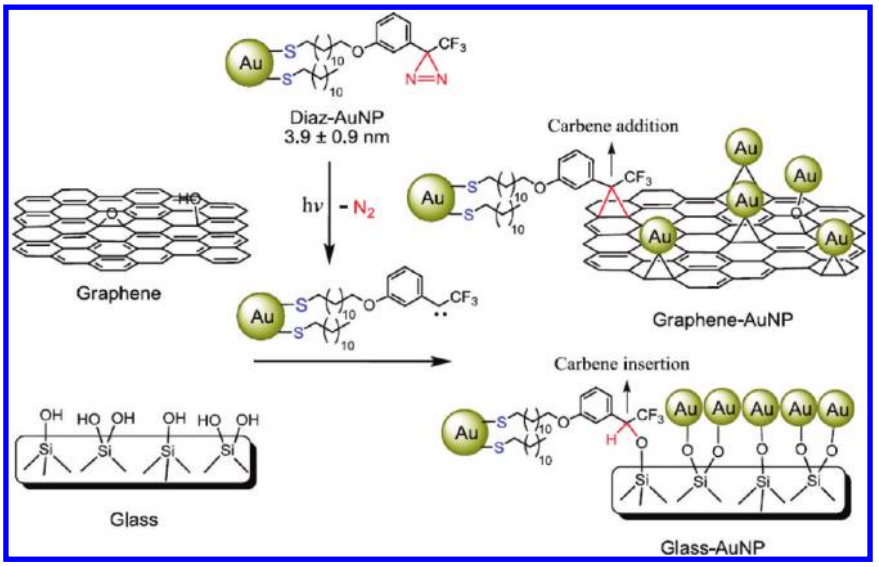

(adventitious carbon) set to 284.8 eV. Spectra were analyzed using Casa XPS software (version 2.3.14). The atomic force microscopy (AFM) images were obtained using tapping mode in ambient conditions with a Multimode AFM (Veeco Metrology) equipped with a Nanoscope V controller (Veeco). Si probes (VISTA probes, force constant 40 N/m, resonant frequency 300 kHz) were used. Before the imaging, the gold nanoparticle samples were allowed to dry under ambient conditions for 3 days.

Synthesis of Graphene. Natural graphite was used as the starting material. Graphene was prepared by the oxidation of natural graphite powder using the modified Hummers' method.[44−46] Typically, graphite powder (1 g) and sodium nitrate (0.75 g) were first stirred in concentrated sulphuric acid (37.5 mL) while being cooled in an ice bath. Next, potassium permanganate (4.5 g) was gradually added to form a new mixture. After 2 h in an ice bath, the mixture was allowed to stand for 5 days at room temperature with gentle stirring. Thereafter, 100 mL of 5 wt % sulphuric acid aqueous solution was added into the above mixture over 1 h with stirring. Next, 3 g of hydrogen peroxide (30 wt % aqueous solution) was added to the above mixture and was stirred for 2 h. After that, the suspension was filtered and washed until the pH value of the filtrate was neutral. The slurry, so-called graphite oxide, was dried in a vacuum oven at 60 °C. Next, the graphite oxide was heated at 1050 °C for 30 s under argon to get reduced graphene. The graphene was characterized using SEM, TEM, XRD, and FTIR (see the Supporting Information).

Piranha Treatment of Glass Slides. Standard microscope slides (VWR) were immersed in a piranha solution (70/30 (v/v) H_2SO_4/30% H_2O_2) overnight at room temperature. (Caution: Piranha solution is an extremely strong oxidant, and the handling of piranha solutions requires special protection equipment including a full face shield and heavy duty rubber gloves.) The slides were then rinsed extensively with Milli-Q water and kept in distilled water until use.

Decoration of Graphene with AuNPs To Yield Graphene−AuNP Hybrids. Graphene (~1 mg) was dispersed in 10 mL of THF using sonication (2 min). A solution of Diaz-AuNP (10 mg in 2 mL of THF) was added to the graphene suspension. The mixture was placed in a Pyrex test tube, degassed with argon for 15 min, and irradiated at wavelengths above 300 nm using a Pyrex filtered medium pressure mercury lamp (Hanovia PC 451050/616750, 450 W) at room temperature for 15 h while stirring. Graphene decorated with AuNPs was isolated by centrifugation. The graphene−AuNP hybrid product was then subjected to exhaustive and repetitive centrifugation and washing cycles using THF, toluene, and chloroform (consistently over the course of 3 weeks) to verify the removal of the excess and unreacted Diaz-AuNPs and to demonstrate the robustness of the material. Two control experiments were carried out: (A) the dispersed graphene was stirred with the Diaz-AuNP in THF in the absence of light for 15 h and then subjected to the same workup procedures as that of the irradiated sample; and (B) a mixture of dodecanethiol modified-AuNP (model-AuNP, i.e., without diazirine ligand) and graphene in THF was irradiated under conditions identical to those described above and then subjected to repetitive centrifugation and washing cycles.

Attachment of AuNPs onto Glass Slides. Piranha-treated glass slides were dried by centrifugation. Untreated glass slides were cleaned with Aqua regia solution and dried prior to use. The glass slides were immersed in a solution of Diaz-AuNPs (5 mg) in THF (20 mL). After the solution was saturated with argon for 15 min, the solution was irradiated using a medium pressure mercury lamp at room temperature for 3 h while stirring. The glass slides were removed and rinsed thoroughly with THF, toluene, and chloroform to remove the unreacted Diaz-AuNPs. Two control experiments were performed: (A) both piranha-treated and untreated glass slides were immersed in a solution of Diaz-AuNPs in THF, stored in the dark (no irradiation) for 3 h, and then thoroughly rinsed with THF, toluene, and chloroform; and (B) both piranha-treated and untreated glass slides were immersed in a solution of model-AuNPs in THF, irradiated for 3 h, and then thoroughly rinsed with THF, toluene, and chloroform.

Crude Patterning of AuNPs on Glass Slide. One side of the piranha-treated glass slide was covered with a photomask with a star shape engraved in it. A film of Diaz-AuNPs was formed on the glass by applying the solution of Diaz-AuNPs dropwise. The glass slide was then irradiated under argon atmosphere at room temperature for 3 h. After the photomask was removed, the glass slide was rinsed thoroughly with several solvents and then sonicated in THF for 30 s.

■ RESULTS AND DISCUSSION

Diazirine-modified AuNPs (Diaz-AuNPs), 3.9 ± 0.9 nm, were prepared according to our reported procedure.[21] Briefly,

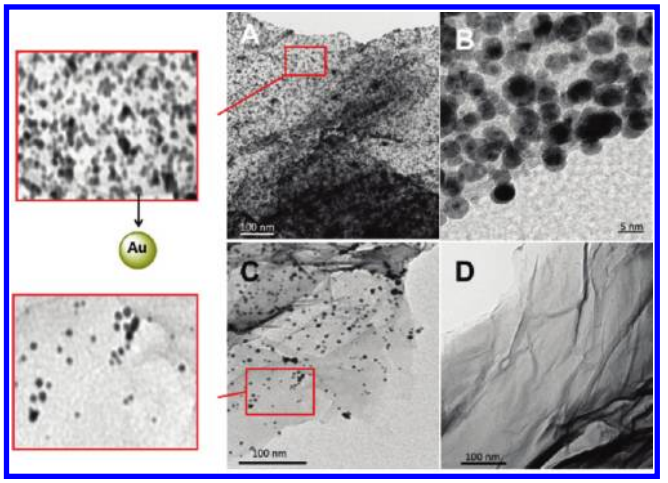

Figure 1. TEM images of (A,B) graphene−AuNP hybrid after washing/purification protocol, (C) graphene after dark/control experiment (in the absence of UV irradiation and after the washing/purification protocol), and (D) unmodified graphene.

tetraoctylammonium bromide (TOAB)-stabilized AuNPs were synthesized by reducing Au^{3+} with $NaBH_4$ in the presence of TOAB. Next, place-exchange of TOABs with 3-aryl-3-(trifluoromethyl)diazirine thiol and dodecanethiol afforded Diaz-AuNPs. The product Diaz-AuNPs were characterized by ^{1}H NMR, ^{19}F NMR, UV−vis spectroscopy, and TEM. The average size of Diaz-AuNPs was 3.9 ± 0.9 nm as determined by TEM. Integration of the relevant signals in the ^{1}H NMR (CH_3 of dodecanethiol and aromatic protons of the diazirine) showed that the ratio of diazirine thiol to dodecanethiol incorporated onto the Diaz-AuNPs is 1:2. Graphene was prepared by the oxidation and exfoliation of graphite powder using the modified Hummers' method.[44−46] The SEM and TEM images (Supporting Information Figures S1 and S2) revealed the wrinkled structure of graphene. The wrinkles are composed of several graphene layers. The XRD spectrum of graphene shows very broad diffraction (002) peak at $2\theta = 26.8°$, indicating the ordered crystal structure of graphene with the extensive conjugated sp^2 carbon networks, while the XRD spectra of graphite oxide and natural graphite powder exhibit the intense peaks at $2\theta = 12°$ (001 plane) and 26.8° (002 plane), respectively (Supporting Information, Figure S3). The peak shift in the latter two is due to the oxidation of natural graphite and increase in the interlayer distance of graphite oxide, respectively. Furthermore, a FTIR study was utilized to monitor the synthesis of graphene (Supporting Information, Figure S4). The FTIR spectrum of natural graphite powder exhibits peaks characteristic of hydroxyl (−OH) and C═C groups. In addition to these peaks, the FTIR spectrum of graphite oxide shows the peaks corresponding to C═O and C−O groups (epoxide and ether), confirming the oxidation of natural graphite. In contrast, only stretching vibrations related to the hydroxyl and C═C groups can be observed in the FTIR of graphene. The disappearance of C═O stretching and weaker intensity of the hydroxyl stretching in the FTIR spectrum of graphene reveal that the greater part of functional groups containing oxygen have been removed (reduced) by heat treatment.[46]

The photochemical approach employed for the covalent decoration of graphene and the glass surface is shown in Scheme 1. As pointed out, upon irradiation (>300 nm) of the diazirine moiety

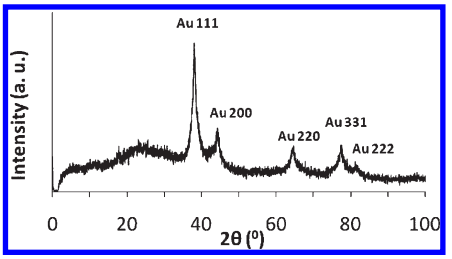

Figure 2. Powder XRD patterns of graphene−AuNP hybrid.

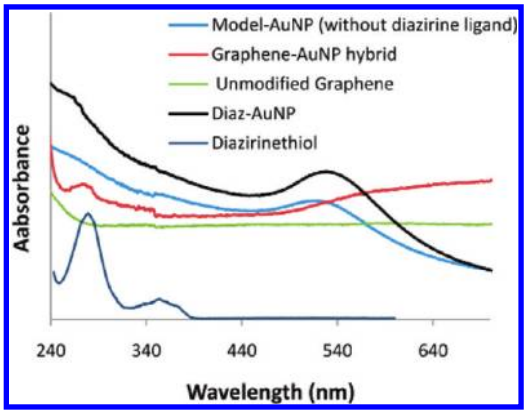

Figure 3. UV−vis absorption spectra of Diaz-AuNPs, model AuNPs, graphene−AuNP hybrid (SPR peak growing at ∼500 nm), unmodified graphene, and diazirinethiol (λ max at 275 nm).

attached to the Diaz-AuNP, a carbene is generated either directly or via secondary photolysis of a diazo-intermediate.[20] Because of the high reactivity of carbene, the carbene nucleophilic addition to C═C bonds of graphene and/or a carbene insertion reaction with hydroxyl groups exposed on the surface of graphene or glass is expected to occur on the basis of our extensive preliminary studies using model OH, COOH, and C═C containing substrates.[20]

To investigate the decoration of graphene with AuNPs, ∼1 mg of graphene was dispersed in 10 mL of THF. Next, a solution of Diaz-AuNPs in THF (5 mg/1 mL) was added to the graphene suspension. The mixture was purged with argon and irradiated using a medium pressure mercury lamp at room temperature for 15 h. The product, a graphene−AuNP hybrid, was isolated by centrifugation. Repeated washing/centrifugation cycles using THF, $CHCl_3$, and toluene were applied to remove any excess or physisorbed Diaz-AuNPs. The solvents utilized in washing/centrifugation cycles dissolve the Diaz-AuNPs; hence the majority of noncovalently attached AuNPs are removed from the graphene surface prior to taking TEM images. Figure 1A and B shows representative TEM and HRTEM images of the graphene−AuNP hybrid, respectively, and the TEM image of the native graphene is shown in Figure 1D. The presence of AuNPs on graphene can be seen in Figure 1A and B, and distribution of AuNPs is very high and fairly even. It is important to mention that AuNPs are stable under our irradiation conditions and no noticeable change in their core size or shape of AuNPs was observed; the size distribution on the composite materials is the same as on the Diaz-AuNP.

The successful fabrication of graphene−AuNP hybrids was further confirmed by powder X-ray diffraction (XRD) analysis. The powder XRD pattern of graphene−AuNP is shown in

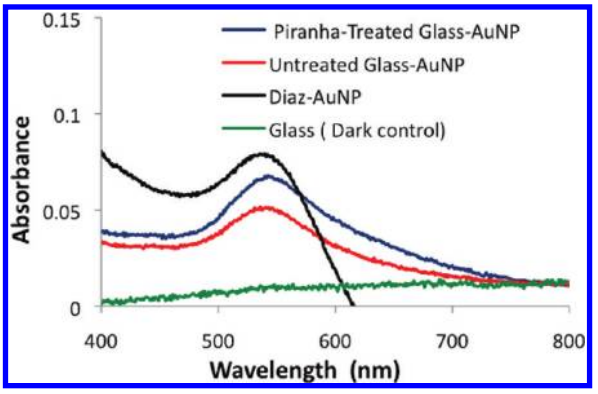

Figure 4. UV−vis absorption spectra of Diaz-AuNPs (SPR peak at 535 nm), untreated glass−AuNP after irradiation (SPR peak at 545 nm), piranha-treated glass−AuNP after irradiation (SPR peak at 550 nm), and of the glass used in the dark control.

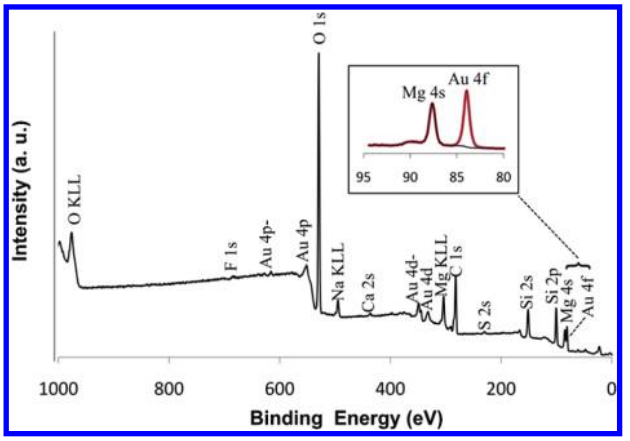

Figure 5. XPS spectrum of piranha-treated glass−AuNP (the inset contains Au 4f and Mg 4s peaks).

Figure 2. The (111), (200), (220), (311), and (222) are planes of a face-centered cubic (fcc) AuNP, confirming the presence of AuNPs in the hybrids. It should be noted that the broad peak centered at $2\theta = 22.8°$ in the XRD of graphene−AuNP hybrids is due to the sample holder (glass) used for the powder XRD measurement.

UV−vis spectroscopy provided further characterization of the graphene−AuNP hybrids (Figure 3). The UV−vis absorption spectrum of Diaz-AuNPs exhibits a weak shoulder at around 275 nm, corresponding to transitions of the incorporated diazirine chromophore onto the AuNP, and a surface plasmon resonance band (SPR) centered at 535 nm, characteristic of AuNPs with a core size >3 nm. As can be observed, the UV−vis absorption of graphene−AuNP hybrids shows the weak shoulder at 270 nm and a very broad growing peak at ∼500 nm. The former absorption peak can be assigned to the diazirine groups bound to the AuNPs in the obtained hybrids, and the latter broad peak is due to the SPR of AuNPs, indicating the presence of the AuNPs in the graphene−AuNP hybrids. It is noteworthy that the decrease in the interparticle distance of AuNPs induces the red shift and broadness in the SPR, and observed SPR of AuNPs in the hybrids is roughly similar to that of aggregated nanoparticles.[47,48]

When the Diaz-AuNP/graphene mixture is not irradiated, the diazirine groups attached onto the AuNPs do not generate a carbene, and therefore no covalent attachment would happen between graphene and Diaz-AuNPs. In this case, if any graphene−AuNP hybrids were formed, only noncovalent interactions between graphene and Diaz-AuNPs would be responsible for them. However, due to the weak nature of noncovalent interactions, AuNPs can be removed from the graphene surface simply by washing with solvent. To test the effect of carbene formation due to irradiation, and subsequent carbene addition onto graphene in forming covalently assembled graphene−AuNP hybrids, a control experiment was carried out. Graphene was dispersed in THF and added to a solution of Diaz-AuNPs in THF and stored in the dark. Next, the mixture was subjected to the same washing/centrifugation protocol to remove the Diaz-AuNPs from the graphene. As can be seen in the representative TEM image Figure 1C, the amount of AuNPs on the graphene is low as compared to those of the irradiated sample (Figure 1A and B) and not uniform. This test supports our contention that AuNPs in the graphene−AuNP hybrids obtained after irradiation are covalently bound to the π-conjugated skeleton and hydroxyl groups of graphene.

The extent of loading can be easily estimated by visual inspection of a series of TEM images like those in Figure 1A and C. For comparison purposes, an area of each of Figure 1A (irradiated) and C (dark/control) is expanded; clearly, the amount of AuNP incorporation on the irradiated samples is more uniform and has a very high concentration of AuNP as compared to the dark sample, which is scattered at best. The few AuNPs remaining on the graphene in the nonirradiated sample may be due to AuNP trapped in defect sites of graphene, making them more difficult to remove with washing or due to some unintentional carbene activation and reactivity with the surface during the lengthy washing procedure. The TEM images of irradiated and nonirradiated samples provided in Figure 1 were taken after extensive and repeated washing/centrifugation cycles. In addition, to verify the need for irradiation in the hybrid formation, a mixture of model-AuNPs (i.e., those without incorporation of the diazirine ligand onto the AuNP but only dodecanethiol ligands, prepared according to previously reported procedure[21]) and graphene was exposed to the same irradiation and purification protocol conditions demonstrated above. The TEM of the obtained material shows only a small amount of AuNP on graphene, less than in Figure 1C and undetectable by the other methods. Again, these are presumably from some physisorption into the layers of the graphene. The conclusion of these control experiments is that UV irradiation of the diazirine moiety in Diaz-AuNP generates the intermediate carbene and its subsequent addition drives the covalently assembled graphene−AuNP hybrid formation. Additional evidence to support that the attachment to the graphene surface is covalent in nature is difficult. Each AuNP needs only one (or a few) carbenes to react with the surface. The remaining (perhaps majority) of the interfacial carbenes generated will simply react with solvent and are essentially wasted. So, while FTIR analysis in principle would provide evidence for the new bonding between the graphene (or glass, vide infra), these signals would be swamped by those of the other trapping products of the carbene that are not required for surface attachment, or other C−C bonds of the other ligands on the AuNP. The high loading of the diazirine onto the AuNP was done to help ensure reaction of the carbene with the surface during its lifetime. After reaction and formation of the hybrid material, the ligands on the AuNP could be place exchanged to incorporate other thiol ligands, including more diazirine thiol to be used for further surface modification.

In a silicate glass surface, Si−O and Si−Si bonds readily react with atmospheric water to form silanol groups (Si−OH); thus

the glass surface is usually hydroxylated.[49] However, to generate more reactive silanol groups on the surface, glass can be treated with piranha solution (H_2SO_4/H_2O_2). We employed both piranha-treated and intact glass slides as potential substrates for AuNP deposition. The glass slides were immersed in a solution of Diaz-AuNPs in THF and irradiated. These were then characterized after thoroughly rinsing the glass slides with several solvents to remove any physisorbed AuNPs. The presence of the AuNP on the glass is apparent visibly (see, for example, Figure 7). UV−vis absorption spectroscopy of the glass−AuNPs formed in the photoreaction is shown in Figure 4. The emergence of the SPR band due to the incorporation of the AuNP in the spectra of piranha-treated and intact glass slides supports the deposition of AuNPs onto the glass surfaces through carbene insertion of Diaz-AUNPs into silanol groups exposed on the glass surface. The SPRs of AuNPs are red-shifted, from 535 nm of unreacted Diaz-AuNPs to 545 and 550 nm of AuNPs on the intact glass−AuNP and piranha-treated glass−AuNP, respectively. Again, these red-shifts are because of interparticle interactions of AuNPs attached onto the glass surfaces. However, the greater red-shift observed in the case of piranha-treated glass−AuNP suggests that the AuNPs are situated closer to each other as compared to those attached to the intact glass surface. Piranha-treated glass has more silanol groups, and thus more Diaz-AuNPs can react with and become attached to the surface.

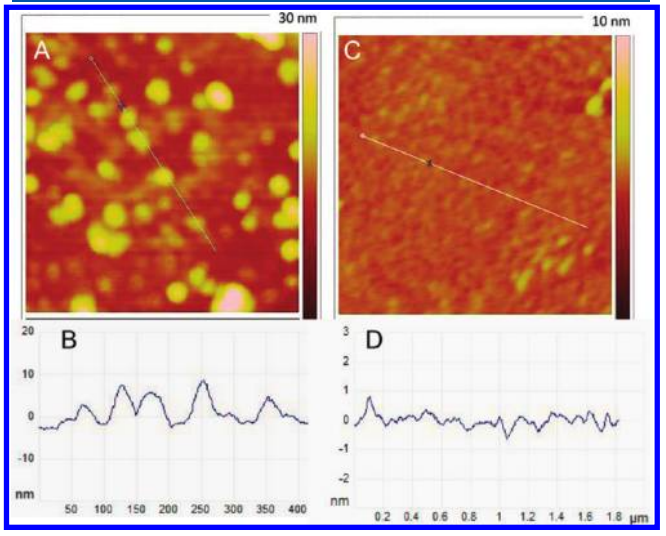

Figure 6. (A) Tapping mode AFM image showing AuNPs covalently deposited onto piranha-treated glass surface, (B) cross-section analysis of AuNPs attached onto the surface, (C) AFM image of piranha-treated glass slide, and (D) cross-section analysis of piranha-treated glass slide.

A control experiment including immersing the piranha-treated glass slide in a Diaz-AuNP solution and storing it in the dark was carried out as well, to ensure the need for irradiation and to determine the role of carbene insertion in the covalent attachment of AuNPs onto the glass surface. After the glass slide was removed and rinsed with solvent, no AuNP was visually evident on the slides, and, more analytically, no SPR was observed in the UV−vis spectrum of the glass slide, indicating the absence of AuNPs on the glass surface (Figure 4). An additional control experiment again revealed that the only role that the UV irradiation plays is to activate the diazirine and generate the carbene at the interface of Diaz-AuNPs. Specifically, piranha-treated glass was immersed in a THF solution of model-AuNPs and irradiated for 3 h. After workup and thoroughly rinsing the glass, there was no observable AuNP attached onto the glass surface visually or by any of the analytical methods.

Further characterization of the glass−AuNP composites was done using X-ray photoelectron spectroscopy (XPS). In addition to the typical peaks of glass, peaks corresponding to Au (4f), Au (4d) and Au (4p), S (2s), and F (1s) are those from the attached AuNPs and confirm the deposition of AuNPs onto the glass (Figure 5).

Atomic force microscopy (AFM) revealed more detail about the glass−AuNP structure. Figure 6A displays the AFM image of piranha-treated glass−AuNP hybrid. The AuNPs are rather closely packed and retain their spherical character. On the basis

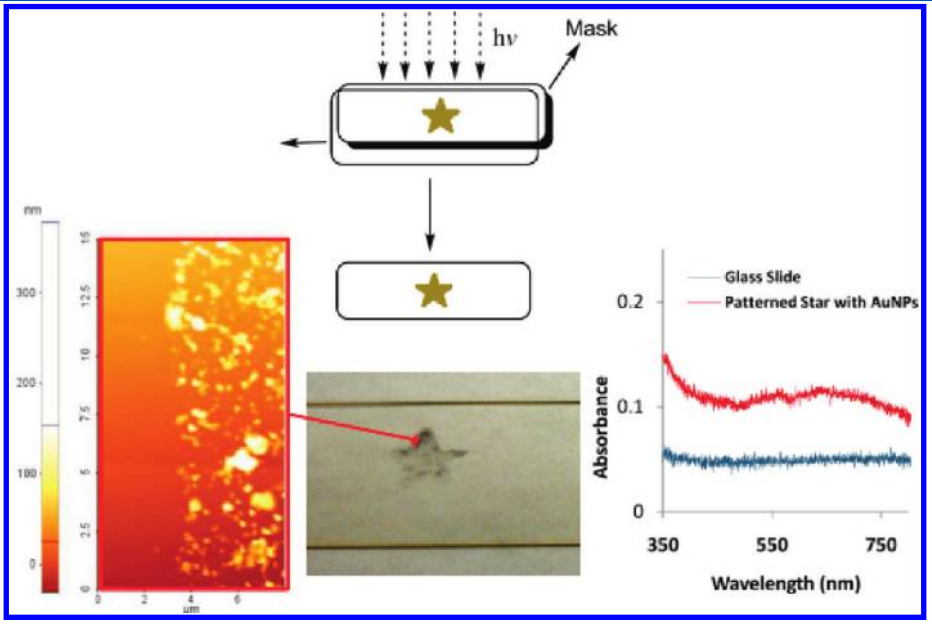

Figure 7. Photograph and cartoon of glass slide showing the AuNP patterned on a piranha-treated glass slide utilizing photoinitiated carbene insertion method.

dx.doi.org/10.1021/la202815g |*Langmuir* 2011, 27, 13261–13268

of the line scan and height profile of AFM images (Figure 6B), the average size of the AuNPs is ~6 ± 0.5 nm, indicating deposition of a thin layer of AuNPs on the glass surface. It should be noted that the TEM analysis gives only the average Au core size of AuNPs and not the actual entire size of AuNPs, which consists of both the size of the Au core and that of the protecting alkane monolayer. The length of the protecting monolayer is approximately 1 nm. By assuming a protecting monolayer between the glass surface and the Au core and another one between the Au core and the AFM tip, the average size of ~6 ± 0.5 nm measured by AFM is in accord with the average Au core size of Diaz-AuNPs (3.9 ± 0.9 nm) measured using TEM. Figure 6C and D shows the AFM and height profile, respectively, of a piranha-treated glass slide.

Because of the chemical inertness and transparency of glass slides, they offer an ideal surface for the fabrication of patterned structures, in particular, by utilizing photochemical approaches. As a visual proof of concept, we demonstrate the macro-patterning of Diaz-AuNPs onto the piranha-treated glass slide. In this simple experiment, a photomask with a star shape engraved in it was placed on the glass surface coated with Diaz-AuNPs. The glass slide was irradiated under argon atmosphere at room temperature. The mask was removed, and the slide was rinsed thoroughly with several solvents and then sonicated in THF for 30 s to remove any unreacted Diaz-AuNPs from the glass surface. Figure 7 shows visibly the assembly of AuNPs on a glass slide in a star shape. Figure 7 also contains an AFM image showing the edge of the star-shaped photomask that illustrates the AuNPs are deposited only where irradiated. Unlike the sample described in Figure 6, which was prepared by irradiation of a glass slide in a solution of the Diaz-AuNP, the sample in Figure 7 was prepared by irradiating a film of AuNP through the mask on the glass slide. In the latter, the AuNP are more aggregated and lead to a higher loading of the AuNP and linking of several AuNPs together via interparticle carbene reactions. On the right is the UV−vis spectrum of the star region showing the SPR band, which supports deposition of the AuNP. Together these results suggest that the method will work for micro- or nanopatterning of glass surfaces.

CONCLUSIONS

The ubiquitous use of the light-activated carbene-modified AuNP protocol for the fabrication of covalently assembled AuNP hybrid materials has been demonstrated on two very different surfaces, the fabrication of graphene−AuNP and glass−AuNP hybrids. Analysis using TEM, powder-XRD, and UV−vis spectroscopy verified the incorporation of high and uniform coverage of AuNPs onto graphene. The composite material resulting from irradiation of the carbene precursor, Diaz-AuNP, in the presence of the graphene is robust enough to survive washing/centrifuge/sonication cycles. The same does not occur in the absence of light. For applications of graphene−AuNP hybrids, like in solar cell development, a high coverage of AunP and its ability for the AuNP to survive centrifugation is favored, and this is achieved effectively by our methodology. In addition, another very important advantage of utilizing our carbene approach is that the reduced graphene, which shows better physical properties in comparison to the graphene oxide, can be employed to fabricate graphene−AuNP hybrid, and there is no need of premodification of the reduced graphene. Similarly, TEM, powder-XRD, XPS, UV−vis spectroscopy, and AFM analysis verified the incorporation of AuNP onto both native (untreated) and piranha solution-treated simple glass slides. The methodology was shown to be suitable for photopatterning.

Because of the high reactivity of the carbene photogenerated at the monolayer of the AuNP in this platform, insertion/addition reactions with virtually any inherent (pre-existing) surface functionality (or that which can be added/enhanced easily by chemical pretreatment) allow the easy photoinduced formation of AuNP-based hybrids. Of course, altering the concentration of the AuNP used or the length of irradiation can also control the extent incorporation of the AuNP onto these materials. While we used AuNP of ca. 4 nm core diameter, the protocol can be extended to smaller and much larger particles that can be modified with our diazirine moiety to deposit nanoparticles onto the surface of a wide variety of materials. While we used a gold nanoparticle as a model functional material to investigate the photoinitiated carbene insertion approach for covalently coupling different two different (nano) materials, this approach using the diazirine moiety certainly can be expanded to use the carbene to decorate target surfaces with a wide variety of other types of nanoparticles (such as silica, quantum dot, and silver nanoparticles) and other functionality. Work to this end is currently underway in our laboratory.

ASSOCIATED CONTENT

Supporting Information. TEM and SEM images of graphene, FT-IR and XRD spectra of natural graphite, graphite oxide, and graphene, ^{1}H NMR spectra of Diaz-AuNPs and diazirinethiol, TEM image of Diaz-AuNPs, and absorption spectra of Diaz-AuNP, model AuNPs, and diazirinethiol. This material is available free of charge via the Internet at http://pubs.acs.org.

AUTHOR INFORMATION

Corresponding Author
*E-mail: mworkent@uwo.ca.

ACKNOWLEDGMENT

This research is supported by the Natural Sciences and Engineering Research Council of Canada discovery and research tools infrastructure grants program (NSERC-DG and NSERC-RTI). Robert Harris at the Advanced Analysis Centre at the University of Guelph (TEM), Richard Harris and Richard B. Gardiner at the Western Biotron (TEM), and Dr. German Popov (XRD) are thanked for their technical expertise. Professor Paul Charpentier is thanked for access to his AFM.

REFERENCES

(1) Nie, Z.; Petukhova, A.; Kumacheva, E. *Nat. Nanotechnol.* **2010**, *5*, 15–25.
(2) Curri, M. L.; Comparelli, R.; Striccoli, M.; Agostiano, A. *Phys. Chem. Chem. Phys.* **2010**, *12*, 11197–11207.
(3) Wang, L.; Luo, J.; Schadt, M. J.; Zhong, C. J. *Langmuir* **2009**, *26*, 618–632.
(4) Sau, T. K.; Rogach, A. L.; Jackel, F.; Klar, T. A.; Feldmann, J. *Adv. Mater.* **2010**, *22*, 1805–1825.
(5) Lim, S. I.; Zhong, C. J. *Acc. Chem. Res.* **2009**, *42*, 798–808.
(6) Kinge, S.; Crego-Calama, M.; Reinhoudt, D. N. *ChemPhysChem* **2008**, *9*, 20–42.
(7) Stewart, M. E.; Anderson, C. R.; Thompson, L. B.; Maria, J.; Gray, S. K.; Rogers, J. A.; Nuzzo, R. *Chem. Rev.* **2008**, *108*, 494–521.

(8) Singh, R.; Premkumar, T.; Shin, J. Y.; Geckeler, K. E. *Chem.-Eur. J.* **2010**, *16*, 1728–1743.
(9) Navalon, S.; Martin, R.; Alvaro, M.; Garcia, H. *Angew. Chem., Int. Ed.* **2010**, *49*, 8403–8406.
(10) Wang, Z.; Ma, L. *Coord. Chem. Rev.* **2009**, *253*, 1607–1618.
(11) Cobley, C. M.; Chen, J.; Cho, E. C.; Wang, L. V.; Xia, Y. *Chem. Soc. Rev.* **2011**, *40*, 44–56.
(12) Aureau, D.; Varin, Y.; Roodenko, K.; Seitz, O.; Pluchery, O.; Chabal, Y. J. *J. Phys. Chem. C* **2010**, *114*, 14180–14186.
(13) Hsieh, S.; Hsieh, C. W. *Chem. Commun.* **2010**, *46*, 7355–7357.
(14) Quinn, B. M.; Dekker, C.; Lemay, S. G. *J. Am. Chem. Soc.* **2005**, *127*, 6146–6147.
(15) Rance, G. A.; Marsh, D. H.; Bourne, S. J.; Reade, T. J.; Khlobystov, A. N. *ACS Nano* **2010**, *4*, 4920–4928.
(16) Liu, X. W.; Mao, J. J.; Liu, P. D.; Wei, X. W. *Carbon* **2011**, 477–483.
(17) Liu, Z.; Jiang, L.; Galli, F.; Nederlof, I.; Olsthoorn, R. C. L.; Lamers, G. E. M.; Oosterkamp, T. H.; Abrahams, J. P. *Adv. Funct. Mater.* **2010**, *20*, 2857–2865.
(18) Kondo, T.; Aoshima, S.; Hirata, K.; Honda, K.; Einaga, Y.; Fujishima, A.; Kawai, T. *Langmuir* **2008**, *24*, 7545–7548.
(19) Weng, J.; Xue, J.; Ye, J. S.; Cui, H.; Sheu, F. S.; Zhang, Q. *Adv. Funct. Mater.* **2005**, *15*, 639–647.
(20) Ismaili, H.; Lee, S.; Workentin, M. S. *Langmuir* **2010**, *26*, 14958–14964.
(21) Ismaili, H.; Lagugné-Labarthet, F.; Workentin, M. S. *Chem. Mater.* **2011**, *23*, 1519–1525.
(22) Ismaili, H.; Workentin, M. S. *Chem. Commun.* **2011**, 7788–7790.
(23) Lawrence, E. J.; Wildgoose, G. G.; Aldous, L.; Wu, Y. A.; Warner, J. H.; Compton, R. G.; McNaughter, P. D. *Chem. Mater.* **2011**, *23* (16), 3740−3751.
(24) Bai, H.; Li, C.; Shi, G. *Adv. Mater.* **2011**, *23*, 1089–1115.
(25) Verdejo, R.; Bernal, M. M.; Romasanta, L. J.; Lopez-Manchado, M. A. *J. Mater. Chem.* **2011**, *21*, 3301–3310.
(26) Pumera, M. *Chem. Soc. Rev.* **2010**, *39*, 4146–4157.
(27) Avouris, P. *Nano Lett.* **2010**, *10*, 4285–4294.
(28) Yang, W.; Ratinac, K. R.; Ringer, S. P.; Thordarson, P.; Gooding, J. J.; Braet, F. *Angew. Chem., Int. Ed.* **2010**, *49*, 2114–2138.
(29) Mohanty, M.; Berry, V. *Nano Lett.* **2008**, *8*, 4469–4476.
(30) Wu, Z. S.; Ren, W.; Wen, L.; Gao, L.; Zhao, J.; Chen, Z.; Zhou, G.; Li, F.; Cheng, H. M. *ACS Nano* **2010**, *4*, 3187–3194.
(31) Zhang, L.; Xia, J.; Zhao, Q.; Liu, L.; Zhang, Z. *Small* **2010**, *6*, 537–544.
(32) Jung, H. J.; Cheon, D. S.; Liu, F.; Lee, K. B.; Seo, T. S. *Angew. Chem., Int. Ed.* **2010**, *49*, 5708–5711.
(33) Huang, J.; Zhang, L.; Chen, B.; Ji, N.; Chen, F.; Zhang, Y.; Zhang, Z. *Nanoscale* **2010**, *2*, 2733–2738.
(34) Myung, S.; Park, J.; Lee, H.; Kim, K. S.; Hong, S. *Adv. Mater.* **2010**, *22*, 2045–2049.
(35) Xiong, Z.; Zhang, L. L.; Ma, J.; Zhao, X. S. *Chem. Commun.* **2010**, *46*, 6099–6101.
(36) Kedem, O.; Tesler, A. B.; Vaskevich, A.; Rubinstein, I. *ACS Nano* **2011**, *5*, 748–760.
(37) Hsu, C. Y.; Huang, J. Y.; Lin, K. J. *Chem. Commun.* **2011**, *47*, 872–874.
(38) Karakouz, T.; Holder, D.; Goomanovsky, M.; Vaskevich, A.; Rubinstein, I. *Chem. Mater.* **2009**, *21*, 5875–5885.
(39) Nath, N.; Chilkoti, A. *Anal. Chem.* **2004**, *76*, 5370–5378.
(40) Jonkheijm, P.; Weinrich, D.; Schroder, H.; Niemeyer, C. M.; Waldmann, H. *Angew. Chem., Int. Ed.* **2008**, *47*, 9618–9647.
(41) Onclin, S.; Ravoo, B. J.; Reinhoudt, D. N. *Angew. Chem., Int. Ed.* **2005**, *44*, 6282–6304.
(42) Hutter, E.; Pileni, M. P. *J. Phys. Chem. B* **2003**, *107*, 6497–6499.
(43) Demko, M. T.; Cheng, J. C.; Pisano, A. P. *Langmuir* **2010**, *26*, 16710–16714.
(44) Hummers, W. S.; Offeman, R. E. *J. Am. Chem. Soc.* **1958**, *80*, 1339–1342.
(45) Hirata, M.; Gotou, T.; Horiuchi, S.; Fujiwara, M.; Ohba, M. *Carbon* **2004**, *42*, 2929–2937.
(46) Schniepp, H. C.; Li, J. L.; McAllister, M. J.; Sai, H.; Herrera-Alonso, M.; Adamson, D. H.; Prud'homme, R. K.; Car, R.; Saville, D. A.; Aksay, I. A. *J. Phys. Chem. B* **2006**, *110*, 8535–8539.
(47) Tan, J.; Liu, R.; Wang, W.; Liu, W.; Tian, Y.; Wu, M.; Huang, Y. *Langmuir* **2010**, *26*, 2093–2098.
(48) Wang, T.; Hu, X.; Qu, X.; Dong, S. *J. Phys. Chem. B* **2006**, *110*, 6631–6636.
(49) Doremus, R. H. J. *Glass Science*; Wiley & Sons: New York, 1994.